Extended Frequency Bandwidth and Electrical Resonance Tuning in Hybrid Terfenol-D/PMN-PT Transducers in Mechanical Series Configuration

PATRICK R. DOWNEY AND MARCELO J. DAPINO*

Department of Mechanical Engineering, The Ohio State University, Suite 224, 650 Ackerman Road, Columbus, OH 43210, USA

ABSTRACT: This article addresses the modeling and characterization of hybrid transducers incorporating both ferroelectric and ferromagnetic elements. The complementary electrical and mechanical properties of the two classes of materials can yield transducers with higher performance or enhanced functionality relative to single-element devices. As a template for studying the properties of hybrid architectures, a transducer is considered which consists of a mechanical series arrangement of a PMN-PT stack and a Terfenol-D rod. This configuration exhibits a double resonant frequency response that can be tuned for a variety of applications. We are specifically interested in the development of models and design criteria for achieving broadband electromechanical transduction over the range from 500 Hz to over 6 kHz. To that end, a model is presented which is constructed from three classical, widely available theories: (i) linear mechanical vibrations, (ii) classical electroacoustics, and (iii) linear piezoelectricity and piezomagnetism. Despite the general limitations of linear models when applied to nonlinear materials, the linear formulation is justified in this article by the consideration of biased, low signal regimes in which transducer behavior is quasilinear. The model is applicable to the design and control of high-performance devices, while being mathematically tractable and accurate over the regimes considered. The model also provides a framework which permits extraction of material property information from dynamic impedance measurements – as opposed to quasistatic measurements – that is under conditions similar to those found in transducer operation. The study also shows that it is possible to tune the electrical resonance frequency without fundamentally altering the transducer bandwidth. This result has practical implications in that it allows matching of the transducer response to individual drivers. This could allow for retrofit of an existing hybrid device with a newer, more advanced ferroelectric stack without compromising the device bandwidth.

Key Words: PMN-PT, Terfenol-D, hybrid transducer, broadband transduction, linear models, electrical tuning.

INTRODUCTION

CONVENTIONAL smart material transducers employ a single drive element for actuation or sensing. The complementary mechanical and electrical properties of ferroelectric and ferromagnetic materials can be employed effectively to design hybrid transducers with enhanced performance or added functionality compared with single-element devices. Specifically in the area of acoustic transduction, performance metrics that have been targeted for improvement by means of hybrid designs include energy efficiency, coupling coefficient, projector directionality and frequency bandwidth.

The principle for achieving high energy efficiency in an electromechanical transducer is that more mechanical output can be produced with less electrical energy if the available reactive energy is shared between capacitive and inductive components. In hybrid ferroic transducers, the ferroelectric material provides the capacitance while the ferromagnetic material provides the inductance. Janocha and Clephas (1996) implemented this principle in an unusual inchworm actuator which consists of two main components, a fixed magnetostrictive rod and a moving assembly that houses two piezoelectric clamps and a coil for driving the magnetostrictive rod. Despite the theoretical advantages of this design, the resonant frequency of the drivers is not self-tunable and varies significantly with the mechanical load, making this type of hybrid architecture difficult to drive efficiently.

A related metric that has been targeted for improvement is the coupling coefficient k, which for a given material is defined as the square root of the ratio of mechanical energy stored (or converted) to total energy stored. The theoretical effective coupling k_e of a hybrid

*Author to whom correspondence should be addressed.
E-mail: dapino.1@osu.edu

1045-389X/05/09 0757–16 $10.00/0 DOI: 10.1177/1045389X05055000

piezoelectric/magnetostrictive transducer relative to the individual piezoelectric and magnetostrictive sections has been shown to respectively increase from 0.52 to 0.60 (18%) and 0.42 to 0.60 (43%) (Butler et al., 1996). In practice, a self-tuning Terfenol-D/PZT-4 transducer was shown to have an effective coupling coefficient 25% greater than that of conventional Tonpilz type transducers (Butler, 1998).

Underwater piston-type projectors with large front-to-back ratio are desirable for increasing the directionality of the acoustical signals. The enhancement of motion at one end and cancelation at the opposite end is achieved by means of a double resonant, half-wavelength design, which exploits the intrinsic 90° phase difference between magnetostrictive and piezoelectric velocities. This phase difference is combined with an additional 90° phase shift due to time delays in the transducer to allow for mechanical unidirectionality as described in Butler and Clark (1984), Butler et al. (1990), and Butler et al. (1993).

Frequency bandwidth is the fourth metric that has been addressed for improvement through hybrid architectures. It has been shown that hybrid actuators can produce increased velocity output in the low frequency range when compared with conventional devices. Butler and Tito (2000) presented an underwater projector which follows the mechanical series arrangement of a magnetostrictive and a piezoelectric section originally proposed by Butler and Clark (1984), but in which the ratio of tail, center and head masses has been optimized for increased frequency bandwidth rather than unidirectional operation. As in devices optimized for large front-to-back pressure ratios, key properties that facilitate the improved bandwidth in this transducer are an inherent 90° phase shift between the velocities of the two sections and a natural difference in the speed of sound in the two materials. In addition, under certain drive conditions the complementary electrical properties of each section results in transducer electrical self tuning. The transducer generates over 1 kHz of extra bandwidth on the low frequency range, and the directionality was addressed by incorporating 16 transducers into a 4×4 element planar array. Modeling of the individual elements was based on an electrical equivalent circuit formulation and on proprietary finite element analysis, while mathematical modeling of the array was based on Pritchard's interaction theory for pistons in a rigid baffle.

This article is focused on obtaining enhanced frequency bandwidth through a mechanical series arrangement of ferroelectric and ferromagnetic sections, which are electrically connected in parallel. Unlike in prior studies, the ferroelectric material is lead magnesium niobate ($Pb(Mg_{1/3}Nb_{2/3})O_3$) doped with lead titanate ($PbTiO_3$) for enhanced linearity and high electrostriction. The ferromagnetic section employs a cylindrical Terfenol-D rod. The model presented here differs from that by Butler and Tito (2000) in that the electromechanical transducer equations are expressed in terms of the applied voltage rather than force terms representing the actuation forces produced by the individual sections. This permits direct correlation of the model with physical transducer inputs. In addition, in our design the Terfenol-D resonance has been placed lower than in Butler and Tito (2000), allowing enhanced response in the low frequency range below 1 kHz.

The models developed in this study also permit extraction of material properties from dynamic impedance measurements, as opposed to the more conventional approach of using quasistatic characterization techniques. Our characterization approach facilitates the collection of material property information under conditions similar to those found in dynamic transducer operation. The difference between the dynamic and quasistatic method is significant if one considers, for instance, that while the strain produced by Terfenol-D exhibits a butterfly shaped curve at quasistatic frequencies, it takes on an elliptic shape tilted at various angles as the frequency is increased. The piezomagnetic coefficients derived through either method will be significantly different. The model is thus developed with the dual goals of device design and material characterization in mind. To that end, the model comprises three main sets of equations: (i) mechanical vibrations equations for the transducer; (ii) equations for the individual active elements derived from classical electroacoustics theory which relate the applied voltages to the ensuing forces; and (iii) constitutive equations for the active elements which provide relationships between measured material properties and the electromechanical transduction coefficients developed in steps (i) and (ii). Combination of the three sets of equations expressed in the frequency domain yields expressions for the electrical impedance and head mass velocity.

It is emphasized that while the model is linear, the approach is justified by the fact that both sections are driven in regimes where the behaviors can be considered linear. Doped PMN-PT exhibits linear electrostriction when driven with a suitable bias field. The Terfenol-D section is magnetically biased and driven at linear regimes far below saturation to avoid cracking of the rod due to inertial forces stemming from the mechanical load. Both sections are operated under a mechanical preload. The accuracy of the results is substantiated by means of experimental measurements collected from a research transducer developed for purposes of model parameter identification and validation. The measurements reflect excellent agreement between modeled and physical behaviors.

The study also reveals that it is possible to tune the electrical resonance frequency without fundamentally altering the transducer bandwidth. Our measurements

show that the PMN-PT section can behave inductively when coupled with the Terfenol-D section due to the mobility loop being located in the first quadrant and the PMN-PT resonance located below the electrical resonance frequency. By wiring a suitable external capacitor in parallel with the circuit, the electrical resonance frequency is forced to lie in between the Terfenol-D and PMN-PT resonances such that the two sections behave as expected, as an inductor and a capacitor. We show that for this particular transducer design, the electrical tuning does not affect the device bandwidth. The latitude for tuning the device capacitance can be regarded as an additional degree of freedom which can be used to match the transducer bandwidth to drivers of different capacitance. Variations in driver capacitance are expected in commercial grade material, even among elements of the same nominal composition, and among different ferroelectric materials. This could have important implications in terms of retrofitting existing devices with new materials.

THEORY

A coupled model describing the electrical and mechanical regimes of the transducer shown in Figure 1 is presented. The model is formulated in three steps. In the first, linear mechanical vibrations theory is used to represent the mechanical impedance transfer function for each material section. In the second modeling step, classical electroacoustics theory is used to describe the coupling between mechanical and electrical regimes and to identify pertinent physical system parameters. In the third step, we develop expressions for all of the coefficients in the electroacoustics framework in terms of material properties of the active elements. This involves the development of constitutive equations relating stress, strain, and magnetic field. The resulting set of equations yields expressions for the spectrum of the head mass velocity and the electrical impedance transfer function.

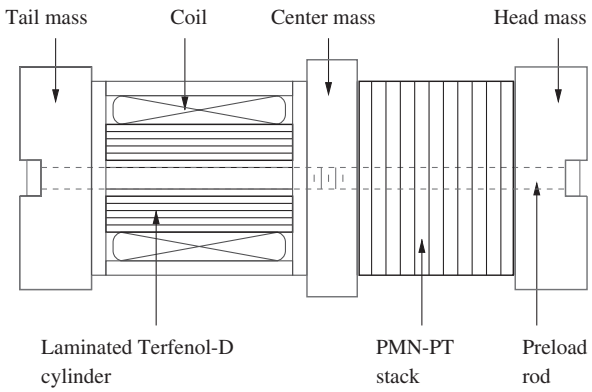

Figure 1. *Tonpilz-type hybrid ferroelectric/ferromagnetic transducer.*

Mechanical Model

The transducer architecture employed here consists of a mechanical series arrangement of a PMN-PT and a Terfenol-D section joined through a rigid center mass, with oscillating head and tail masses at opposite ends. This configuration provides a double resonant frequency response which is used to facilitate broad frequency bandwidth operation. For modeling purposes, each active material is assumed to behave mechanically as a tunable compliance arranged in parallel with a damper, as described by the three degree of freedom linear vibratory system shown in Figure 2.

The equation of motion for each mass is expressed in the frequency domain and written in terms of the velocity vector $\boldsymbol{v}$ as

$$\left([\mathbf{M}]s + [\mathbf{C}] + [\mathbf{K}]\frac{1}{s}\right)\boldsymbol{v} = \boldsymbol{F}, \tag{1}$$

where the structural matrices and vectors are defined as

$$[\mathbf{M}] = \begin{bmatrix} m_1 & 0 & 0 \\ 0 & m_2 & 0 \\ 0 & 0 & m_3 \end{bmatrix}$$

$$[\mathbf{C}] = \begin{bmatrix} r_1 & -r_1 & 0 \\ -r_1 & r_1 + r_2 & -r_2 \\ 0 & -r_2 & r_2 \end{bmatrix}$$

$$[\mathbf{K}] = \begin{bmatrix} 1/c_1 & -1/c_1 & 0 \\ -1/c_1 & 1/c_1 + 1/c_2 & -1/c_2 \\ 0 & -1/c_2 & 1/c_2 \end{bmatrix}$$

$$\boldsymbol{v} = \begin{bmatrix} v_1 \\ v_2 \\ v_3 \end{bmatrix}$$

$$\boldsymbol{F} = \begin{bmatrix} F_1 \\ F_2 - F_1 \\ -F_2 \end{bmatrix}.$$

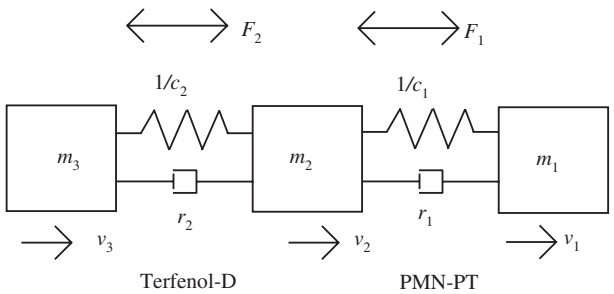

Figure 2. *Lumped parameter vibratory model representing the hybrid actuator.*

Here, m represents the mass, r the damping coefficient, c the mechanical compliance, v the velocity, F the force, and s the Laplace derivative operator $j\omega$. The subscripts 1 and 2 on the applied forces, damping elements and compliances respectively denote the PMN-PT and Terfenol-D sections. The subscripts 1, 2, and 3 on the velocity vector respectively denote the head, center, and tail masses.

In order to determine the criteria for broadband motion of the head mass, the algebraic system of Equations (1) is solved for v_1 as a function of the forcing functions F_1 and F_2. As a means to fully describe the mechanical regime, the force per velocity transfer function (mechanical impedance function) is found for each material section. To analyze the PMN-PT section, the force F_2 from the Terfenol-D rod is set equal to zero. The resulting impedance F_1/v_1 then takes the form

$$Z_{\text{mech,E}} = \frac{F_1}{v_1} = \frac{As^4 + Bs^2 + C}{sc_1(m_2m_3c_2s^2) + (m_2 + m_3)(r_2c_2s + 1)}. \tag{2}$$

Proceeding in analogous fashion for the Terfenol-D rod one obtains

$$Z_{\text{mech,M}} = \frac{F_2}{v_1} = \frac{As^4 + Bs^2 + C}{sc_2m_3(r_1c_1s + 1)}. \tag{3}$$

The subscripts E and M respectively denote 'electric' and 'magnetic' for the PMN-PT and Terfenol-D elements. In Equations (2)–(3), the terms A, B, and C have the form

$$A = (m_1m_2m_3c_1c_2)$$

$$B = m_3(m_1 + m_2)c_2(r_1c_1s + 1) + m_1(m_2 + m_3)c_1(r_2c_2s + 1)$$

$$C = (r_1c_1s + 1)(r_2c_2s + 1)(m_1 + m_2 + m_3).$$

Relations (2)–(3) are sufficiently general to characterize the transducer's output response due to activation of either smart material given suitable values for the material properties. Consistently with prior work (Butler and Tito, 2000), we have determined that optimum bandwidth is achieved using a head : center : tail mass ratio of approximately 1 : 2 : 2.5, and having the PMN-PT stack stiffness $1/c_1$ be much higher than that of the Terfenol-D rod, $1/c_2$. Using these mass values, the transducer output can be approximated by two dominant modes, the third being a zero-frequency rigid translation. The PMN-PT stack controls the upper resonance where the tail mass essentially decouples from the system and the head and center masses vibrate out of phase with each other. This case is illustrated in Figure 3(b) and described by the relations

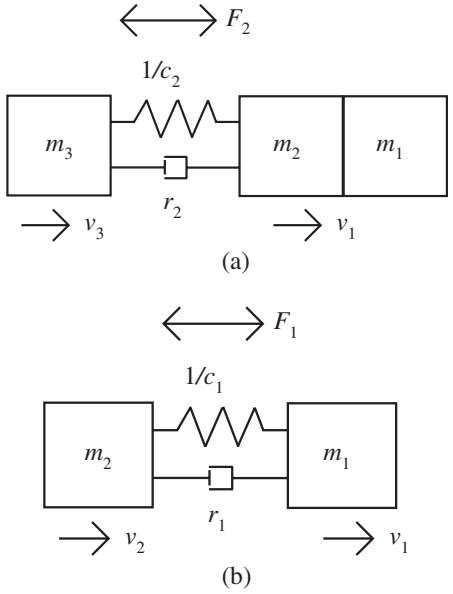

Figure 3. *Mechanical representation of the simplified vibratrion modes at (a) low frequencies (Terfenol-D) and (b) high frequencies (PMN-PT).*

$$\left(m_1s + r_1 + \frac{1}{sc_1}\right)v_1 = F_1 + \left(r_1 + \frac{1}{sc_1}\right)v_2 \tag{4}$$

$$\left(m_2s + r_1 + \frac{1}{sc_1}\right)v_2 = -F_1 + \left(r_1 + \frac{1}{sc_1}\right)v_1. \tag{5}$$

The lower resonance is controlled by the Terfenol-D section and is characterized by the head and center masses lumped together vibrating out of phase with the tail mass. This situation is illustrated in Figure 3(a) and described by the relations

$$\left[(m_1 + m_2)s + r_2 + \frac{1}{sc_2}\right]v_1 = F_2 + \left(r_2 + \frac{1}{sc_2}\right)v_3 \tag{6}$$

$$\left(m_3s + r_2 + \frac{1}{sc_2}\right)v_3 = -F_2 + \left(r_2 + \frac{1}{sc_2}\right)v_1. \tag{7}$$

Figure 4 shows head mass velocity calculations based on the full model (1) as well as the two idealized models (4)–(5) and (6)–(7) for the individual smart material sections. A procedure analogous to that employed when formulating relations (2)–(3) yields the following expressions for the mechanical impedances of the PMN-PT stack and Terfenol-D rod

$$Z_{\text{m,E}} = \frac{m_1m_2c_1s^2 + (r_1c_1s + 1)(m_1 + m_2)}{m_2c_1s}, \tag{8}$$

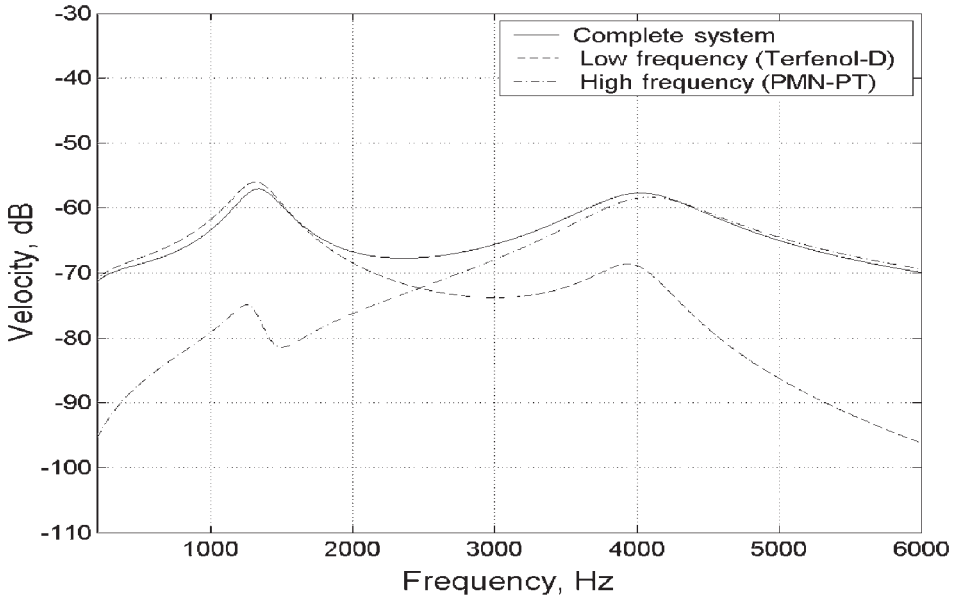

Figure 4. *Head mass velocity response of the complete system as represented by relation (1), and individual responses calculated from the mechanical relations (4)–(5) and (6)–(7).*

$$Z_{\mathrm{m,M}} = \frac{(m_1 + m_2)m_3 c_2 s^2 + (r_2 c_2 s + 1)(m_1 + m_2 + m_3)}{m_3 c_2 s}. \tag{9}$$

These expressions therefore represent the mechanical impedances for the idealized, decoupled modes of vibration that result when the mass ratios and stiffnesses satisfy the conditions stated above. In practice, however, broadband excitation of one section will cause some response in the other, thus altering the location of the independent mass responses relative to the resonances of the combined system (see Figure 4).

Electroacoustics Model

Classical electroacoustic transduction theory (Hunt, 1982) is now considered for the purpose of coupling the vibratory model with the electrical regime. Considering the transduction model for general electromechanical transducers shown in Figure 5, two coupled relations can be written that describe the electrical and mechanical regimes. Assuming linearity, the expressions relating these two regimes are

$$V = Z_{\mathrm{e}} I + T_{\mathrm{em}} v \tag{10}$$

$$F = T_{\mathrm{me}} I + Z_{\mathrm{m}} v, \tag{11}$$

where V is the voltage across the transducer terminals, I is the current flow through the transducer, v is the velocity, F is the force, Z_{e} and Z_{m} respectively denote the blocked electrical and mechanical impedances, and T_{em} and T_{me} are coefficients that describe the electromechanical transduction. The subscripts em and me

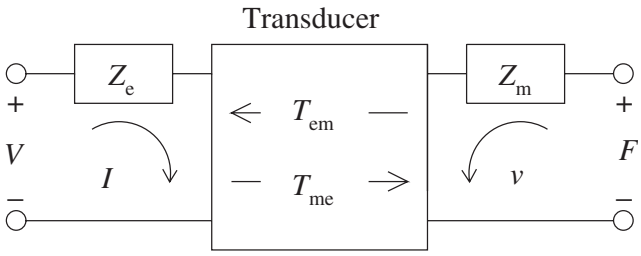

Figure 5. *Four-pole transduction model for electromechanical systems (Hunt, 1982).*

respectively denote 'electrical due to mechanical' and 'mechanical due to electrical' energy transduction processes.

Certain properties of the electromechanical interaction can be studied by considering the driving-point impedance at the electrical terminals, which is the complex ratio of voltage to current. For a general system described by the electroacoustic equations (10)–(11), it is assumed that the force F acts on a load of impedance Z_{L}, which allows Equation (11) to be written in the form

$$v = \frac{-T_{\mathrm{me}} I}{Z_{\mathrm{m}} + Z_{\mathrm{L}}}. \tag{12}$$

Substitution of this equation in Equation (10) gives the total electrical impedance transfer function

$$Z_{\mathrm{ee}} = \frac{V}{I} = Z_{\mathrm{e}} + \frac{-T_{\mathrm{em}} T_{\mathrm{me}}}{Z_{\mathrm{m}} + Z_{\mathrm{L}}} = Z_{\mathrm{e}} + Z_{\mathrm{mot}}. \tag{13}$$

The total electrical impedance is composed of a blocked component Z_{e} equal to the ratio between voltage and current as the transducer is prevented to displace, and a motional component Z_{mot} associated with the

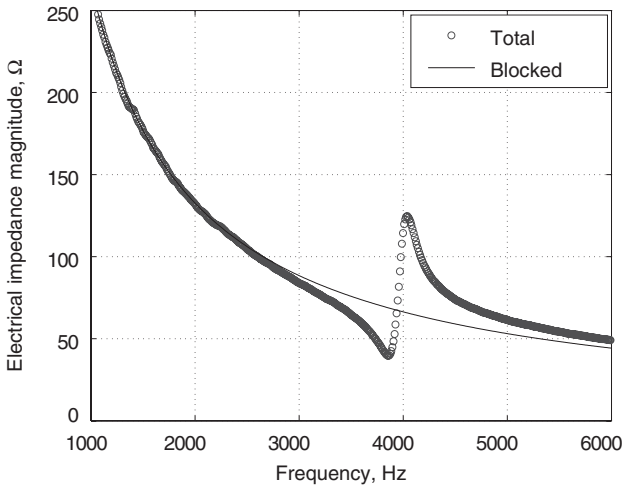

Figure 6. *Magnitude of the total and blocked electrical impedance frequency response function for the PMN-PT section employed in this study.*

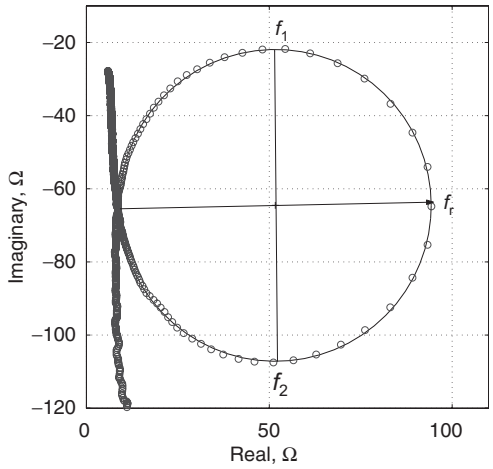

Figure 7. *Experimental impedance loop corresponding to the measurements in Figure 6. The solid lines overlaid on the data show the electrical resonance frequency (f_r) and corresponding half power frequencies f_1 and f_2.*

mechanical motion of the transducer and load. The effects of motional contributions on the measured electrical impedance of the PMN-PT stack employed in this study are illustrated in Figure 6. It is observed that the difference between the total and blocked impedance is larger near the resonance and antiresonance frequencies due to the coupling between motional and electrical regimes. In other words, Z_{mot} provides a measure of the amount of electromechanical coupling in the transducer.

This can be seen more clearly in Figure 7, which shows the Nyquist plot of the same electrical impedance measurements of Figure 6. The electrical resonance frequency f_r is determined from the principal diameter of the Nyquist loop. In general, this resonance does not correspond to the peak in the magnitude of Z_{ee} due to the phase shift not being exactly zero. Physically, the nonzero phase shift is explained by the presence of energetically dissipative terms in the complex transduction coefficients T_{em} and T_{me}. The two points on the circle at 90° from the principal diameter are the half power frequencies f_1 and f_2.

It is emphasized that the impedance function and its inverse, the admittance function $Y_{ee} = 1/Z_{ee}$, provide *different* measures of transducer figures of merit such as coupling coefficients, quality factors, elastic moduli, and sound speeds (Hunt, 1982; Downey et al., 2003; Dapino et al., 2004). Indeed, although the total impedance and admittance functions are the inverse of one another, the coupled motional effects are not, i.e., $Y_{\text{mot}} \neq 1/Z_{\text{mot}}$. One difference between these functions is that in the admittance loop the frequency opposite the crossover point is the antiresonance frequency f_{ar} rather than f_r. Similarly, the points at 90° from f_{ar} are the half power points associated with antiresonance, f_{a1} and f_{a2}. As detailed for Terfenol-D (Dapino et al., 2004), the resonant and antiresonant frequencies quantify the effective coupling coefficient through the relations

$$k_{\text{eff}}^2 = \begin{cases} 1 - \left(\dfrac{f_{ar}}{f_r}\right)^2, & \text{if } f_{ar} < f_r \\ 1 - \left(\dfrac{f_r}{f_{ar}}\right)^2, & \text{if } f_{ar} > f_r \end{cases} \tag{14}$$

which respectively apply to PMN-PT and Terfenol-D. In conjunction with the system masses, the resonance and antiresonance frequencies offer a means of calculating the stiffness of each drive element. From the idealized expressions for mechanical impedance, Equations (8) and (9), the stiffness is determined by setting the imaginary component equal to zero and rearranging,

$$k_m^E = \frac{1}{c_1} = \frac{(2\pi f_r)^2 m_1 m_2}{m_1 + m_2},$$
$$k_m^M = \frac{1}{c_2} = \frac{(2\pi f_r)^2 (m_1 + m_2) m_3}{m_1 + m_2 + m_3}.$$

Here, the superscripts E and M respectively denote the PMN-PT (electric field) and Terfenol-D (magnetic field) sections. These expressions provide a good approximation of the stiffnesses when compared to the values obtained from the full impedances (2)–(3). Assuming linearly elastic behavior, the Young's moduli of the PMN-PT and Terfenol-D drivers are respectively given by

$$E_y^E = \frac{k_m^E L_{e,1}}{A_1}$$
$$E_y^M = \frac{k_m^M L_{e,2}}{A_2},$$

where L_e and A (with appropriate subindices) denote length and cross-sectional area of each active element. The intrinsic sound speeds are subsequently calculated as

$$c_E = \sqrt{\frac{E_y^E}{\rho_E}}$$

$$c_M = \sqrt{\frac{E_y^M}{\rho_M}}$$

where ρ_E and ρ_M denote the material densities.

The electrical impedance and admittance measurements allow the direct determination of the mechanical quality factor of each section,

$$Q_r = \frac{f_r}{f_2 - f_1} \tag{15}$$

$$Q_{ar} = \frac{f_{ar}}{f_{a2} - f_{a1}}. \tag{16}$$

Since each section has two values for Q, the average value is used for transducer design and model validation. By inspection of the mechanical equations of motion, the internal damping is estimated by

$$r_1 = \frac{2\pi f_r m_1 m_2}{Q(m_1 + m_2)} \tag{17}$$

$$r_2 = \frac{2\pi f_r (m_1 + m_2) m_3}{Q(m_1 + m_2 + m_3)} \tag{18}$$

respectively for the PMN-PT and Terfenol-D sections. The above equations relating experimental measurements to transducer figures of merit were employed in this study to determine the model parameters for each section. Measured and calculated properties utilized here are shown in Table 1.

Table 1. Measured material and design parameters of the hybrid actuator.

Terfenol-D	PMN-PT
$k_m^M = 29.3$ N/m	$k_m^E = 136.2$ N/m
$E_y^M = 43.8$ GPa	$E_y^E = 22.57$ GPa
$q = 4.96 \times 10^{-9}$ m/A	$d = 3.08 \times 10^{-10}$ m/V
$r_2 = 486$ Ns/m	$r_1 = 237$ Ns/m
$\mu^\sigma = 6.28 \times 10^{-6}$ H/m	$\varepsilon_0 = 3.25 \times 10^{-8}$ F/m
$L_{block} = 5.2$ mH	$C_{block} = 603$ nF
$k_2 = 0.415$	$k_1 = 0.279$
$n = 25{,}000$ turns/m	$N = 62$ layers
Dia. = 6.4 mm	Dia. = 16 mm
$L_{e,2} = 50.8$ mm	$L_{e,1} = 35.2$ mm
Prestress 6.9 MPa	Prestress 13.8 MPa
Head mass $m_1 = 308$ g, Dia. 76.2 mm, Thick. 26.2 mm	
Center mass $m_2 = 670$ g, Dia. 76.2 mm, Thick. 15.2 mm	
Tail mass $m_3 = 777$ g, Dia. 76.2 mm, Thick. 18.8 mm	

Constitutive Electroacoustic Relations

The electroacoustic relations developed in the previous section provide a framework, which is sufficiently general, to analyze a variety of electromechanical systems. However, in these relations no distinction has been made between ferroelectric and ferromagnetic behavior, which is particularly distinct in terms of the phase between velocity and applied voltage. To address this limitation, the electroacoustic relations (10)–(11) are combined with constitutive equations which describe the strain and polarization produced by the active materials. This will allow for the blocked impedances and transduction coefficients to be expressed in terms of material properties and design parameters for each section.

TERFENOL-D SECTION

Assuming biased operation about low field inputs, we first consider linear piezomagnetic constitutive relations for a Terfenol-D rod driven along the longitudinal '33' direction,

$$\varepsilon = \frac{\sigma}{E_y^M} + qH \tag{19}$$

$$B = q^*\sigma + \mu^\sigma H. \tag{20}$$

Here, ε is the strain, σ is the axial stress, H is the magnetic field, B is the magnetic flux density, μ^σ is the permeability at constant stress, and $q = q^*$ is a symmetric magnetoelastic coupling coefficient. To convert these expressions into a form compatible with relations (10) and (11), it is assumed that the Terfenol-D rod completely fills an ideal wire solenoid and the magnetic field and current are linearly related. For a solenoid with N turns and cross-sectional area A_2, the flux linkage is $\lambda = N\phi = NBA_2$, where $\phi = BA_2$ is the magnetic flux through the rod. Assuming spatial independence of stress and strain, the strain is related to the displacement x by definition $\varepsilon \equiv x/L_{e,2}$, which can then be expressed as a velocity via a first derivative. The total voltage drop is that of a DC resistance R in series with an electrical inductance. Finally, the axial stress in the rod can be related to the internal force by a ratio of cross-sectional areas. These electromechanical relations are summarized as follows:

$$H = nI$$

$$\varepsilon = \frac{v}{j\omega L_{e,2}}$$

$$\sigma = \frac{F}{A_2}$$

$$V = RI + j\omega NBA_2.$$

Here, parameter n represents the turns ratio of the solenoid, $n = N/L_{e,2}$; both rod and solenoid have length $L_{e,2}$. Substitution of these expressions into Equations (19) and (20), and subsequent rearrangement yields (Hall, 1994)

$$V = [R + j\omega\mu^{\sigma}(1 - k_{\text{eff}}^2)n^2 A_2 L_{e,2}]I + Nqk_{\text{m}}^{\text{M}} v, \quad (21)$$

$$F = -Nqk_{\text{m}}^{\text{M}} I + \frac{k_{\text{m}}^{\text{M}}}{j\omega} v. \quad (22)$$

Comparison of these equations with the general electroacoustic relations (10)–(11) gives

$$Z_{\text{e, M}} = R + j\omega\mu^{\sigma}(1 - k_{\text{eff}}^2)n^2 A_2 L_{e,2} = R + j\omega L_{\text{block}}, \quad (23)$$

where L_{block} is defined as $\mu^{\sigma}(1 - k_{\text{eff}}^2)n^2 A_2 L_{e,2}$. This indicates that the blocked electrical impedance $Z_{\text{e,M}}$ for the Terfenol-D section can be represented by an ideal resistor in series with an inductor L_{block} which can be directly determined from measured material properties.

Equations (21) and (22) also determine the transduction coefficients T_{em} and T_{me}. These terms describe the coupling between the electrical and mechanical regimes and can be related to material properties by

$$T_{\text{em, M}} = Nqk_{\text{m}}^{\text{M}} \quad (24)$$

$$T_{\text{me, M}} = -Nqk_{\text{m}}^{\text{M}} = -T_{\text{em, M}}. \quad (25)$$

It is observed that $T_{\text{em, M}}$ and $T_{\text{me, M}}$ are equal in magnitude while opposite in sign. As shown by Hunt (1982), this antisymmetric relationship is expected of all magnetostrictive transducers because of the spatial orthogonality of current and magnetic field. The final electroacoustic coefficient is the blocked mechanical impedance $Z_{\text{m,M}}$. Comparison of Equation (22) with Equation (11) gives $Z_{\text{m, M}} = k_{\text{m}}^{\text{M}}/j\omega$, which contains only a stiffness term due to other dynamic effects such as inertia and damping being tacitly ignored in the constitutive material relations. Due to this discrepancy, the mechanical impedance term derived above is replaced with the more accurate form $Z_{\text{mech, M}}$ given by Equation (3).

PMN-PT SECTION

For low field inputs about a bias field or for materials which exhibit quasilinear behavior, as is the case when this particular PMN-PT stack is operated at room temperature, the constitutive behavior of individual layers can be approximated by the linear piezoelectric constitutive relations, which in strain-charge form are given by

$$\varepsilon = \frac{\sigma}{E_{\text{y}}^{\text{E}}} + \text{d}E \quad (26)$$

$$D = d^{*}\sigma + \epsilon^{\sigma}E, \quad (27)$$

where E is the electric field, D is the electric charge density, E_{y}^{E} is the Young's modulus at constant field, ϵ^{σ} is the electric permittivity at constant stress, and $d = d^{*}$ is a symmetric electroelastic coupling coefficient. In order to develop the expressions that quantify the relationship between the electrical and mechanical domains in electrostrictive materials, we note that for each individual layer in the stack, the voltage is applied across the thickness t of the material, implying that the electric field is equal to V/t. The electric displacement D is defined as charge per unit area and is thus converted into current through $q = I/j\omega$. As before, the assumption of spatially uniform stress and strain in the stack facilitates the development of relations between stress and force, and strain and velocity, as follows

$$E = \frac{V}{t}$$

$$\varepsilon = \frac{v}{j\omega L_{e,1}}$$

$$\sigma = \frac{F}{A_1}$$

$$D = \frac{I}{j\omega A_1}.$$

Here, N is the number of layers in the stack. Substitution of these expressions into Equations (26) and (27), followed by suitable rearrangement yields

$$V = \frac{t}{A_1 j\omega N(\epsilon^{\sigma} - E_{\text{y}}^{\text{E}} d^2)} I + \frac{-\text{d}E_{\text{y}}^{\text{E}}}{j\omega N(\epsilon^{\sigma} - E_{\text{y}}^{\text{E}} d^2)} v \quad (28)$$

$$F = \frac{-\text{d}E_{\text{y}}^{\text{E}}}{j\omega N(\epsilon^{\sigma} - E_{\text{y}}^{\text{E}} d^2)} I + \frac{\epsilon^{\sigma} E_{\text{y}}^{\text{E}} A_1}{j\omega N(\epsilon^{\sigma} - E_{\text{y}}^{\text{E}} d^2)} v. \quad (29)$$

Comparison of these relations with the general electroacoustic relations (10)–(11) indicates that the blocked electrical impedance of the PMN-PT stack is purely capacitive,

$$Z_{\text{e, E}} = \frac{t}{j\omega A_1 N(\epsilon^{\sigma} - E_{\text{y}}^{\text{E}} d^2)} = \frac{1}{j\omega C_{\text{block}}}, \quad (30)$$

where $C_{\text{block}} \equiv A_1 N(\epsilon^{\sigma} - E_{\text{y}}^{\text{E}} d^2)/t$. The two coefficients that characterize the electromechanical transduction can be written from Equations (28) and (29) as

$$T_{\text{em, E}} = \frac{-\text{d}E_{\text{y}}^{\text{E}}}{j\omega N(\epsilon^{\sigma} - E_{\text{y}}^{\text{E}} d^2)} \quad (31)$$

$$T_{\text{me, E}} = \frac{-\text{d}E_{\text{y}}^{\text{E}}}{j\omega N(\epsilon^{\sigma} - E_{\text{y}}^{\text{E}} d^2)}. \quad (32)$$

Consistent with the electrical nature of ferroelectric transduction, and in contrast with the Terfenol-D section, the coefficients are symmetric since they are identical in both magnitude and sign. As for the

Terfenol-D element, the mechanical impedance is solely a compliance term, shown by the $1/j\omega$ dependence in the velocity term of Equation (29). Because the constitutive piezoelectric equations fail to account for all dynamic effects, the expression for the mechanical impedance derived above is replaced with the more complete expression $Z_{\text{mech, E}}$ given by Equation (2).

With all of the electroacoustic coefficients defined in terms of physical parameters, relations (21)–(22) and (28)–(29) are used to calculate the velocity response to an applied input voltage. It is noted that the relationship between applied voltage and velocity is determined by the coefficients $T_{\text{em, M}}$ and $T_{\text{em, E}}$. Comparison of Expressions (24) and (31) reveals that when the two sections are wired in parallel and receive the same input voltage, the phase between the PMN-PT and Terfenol-D velocities always is 90° even when the system moves through resonance, thus ensuring the extended bandwidth of the hybrid transducer (Butler and Tito, 2000).

Combined Linear Transducer Model

Since the PMN-PT and Terfenol-D sections are wired in electrical parallel, their total electrical impedances including motional contributions sum as normal. Thus the transducer's total electrical impedance, incorporating electrical and mechanical effects in both active sections, is

$$Z_{\text{ee, total}} = \frac{Z_{\text{ee, E}} Z_{\text{ee, M}}}{Z_{\text{ee,E}} + Z_{\text{ee, M}}}, \tag{33}$$

in which $Z_{\text{ee, M}}$ is quantified by Equations (13), (23), (24), and (25), and $Z_{\text{ee, E}}$ by Equations (13), (30), (31), and (32).

To quantify the head mass velocity response, first the current in each section is found from the definition of electrical impedance,

$$I_{\text{E}} = \frac{V}{Z_{\text{ee, E}}}$$

$$I_{\text{M}} = \frac{V}{Z_{\text{ee, M}}}$$

where the applied voltage is V for both sections. The velocity contribution from each section is given by Equation (12),

$$v_{\text{E}} = \frac{-T_{\text{me, E}} I_{\text{E}}}{Z_{\text{m, E}} + Z_{\text{L}}}$$

$$v_{\text{M}} = \frac{-T_{\text{me, M}} I_{\text{M}}}{Z_{\text{m, M}} + Z_{\text{L}}}.$$

The final step in the velocity calculations is to recognize that the mechanical series configuration allows for the superposition of the velocities from the two sections, which results in

$$v = v_{\text{E}} + v_{\text{M}}. \tag{34}$$

This also allows for the comparison of the individual section responses by graphing just $Z_{\text{ee,E}}$ and v_{E} or $Z_{\text{ee, M}}$ and v_{M}. Each set assumes no electrical input and thus no excitation of the other section but does account for the coupling due to the attached mechanical components.

EXPERIMENTS

A broadband hybrid transducer was designed and constructed for the purposes of model parameter identification and validation. The magnetostrictive element consists of a monolithic Terfenol-D ($Tb_{0.27}Dy_{0.73}Fe_{1.95}$) rod, 50.8 mm (2 in.) in length and 6.4 mm (0.25 in.) in diameter, manufactured by ETREMA Products, Inc. The field is provided by a 1200 turn coil wound using 26-AWG magnet wire which includes a single layer pick-up coil on the internal diameter. The coil is encased in a cylindrical Alnico V permanent magnet which provides a magnetic bias of 125 Oe (10 kA/m) and is axially slit to reduce eddy currents. The coil resistance is 7.6 Ω. The magnet has inner and outer diameters of 19 mm (0.75 in.) and 35.4 mm (1 in.) and a length of 50.8 mm (2 in.). Machined components of 1018 steel are used to complete a closed magnetic circuit path. The complete magnetic circuit is positioned between the tail mass and the center mass. Each mass is 76.2 mm (3 in.) in diameter and made from non-magnetic stainless steel. The thickness of the head, center and tail mass is respectively 26.2 mm (1.03 in.), 15.2 mm (0.60 in.), and 18.8 mm (0.74 in.), while the respective value of the masses is 308 g (0.7 lb), 670 g (1.5 lb), and 777 g (1.7 lb). Three bolts, each with Belleville washers under the head, are used to compress the magnetic components between the two masses to 6.9 MPa (1 kpsi), with the washers providing a means of applying a consistent compressive prestress to the Terfenol-D rod.

The electrostrictive section employs an EDO Corporation ceramic stack, model EP200-62. The stack composition is lead magnesium niobate (65%) and lead titanate (35%). For this compound, the displacement versus field characteristic is linear at room temperature. The stack consists of 62 individual layers and has a total length of 35.2 mm (1.385 in.) and a diameter of 16 mm (0.63 in.) The ceramic stack is located between the center mass and the head mass. Three prestress bolts with Belleville washers are used to compress the stack to 2.4 MPa (350 psi) and hold the structure together. The complete transducer has a length of 152.4 mm (6 in.) and is shown in Figure 8(a).

The experiments were conducted with the test transducer placed inside of a 76.2-mm-(3 in.)-diameter PVC tube with a neoprene/cork ring around each mass acting as an isolator. The complete assembly was suspended as shown in Figure 8(b) to prevent exogenous

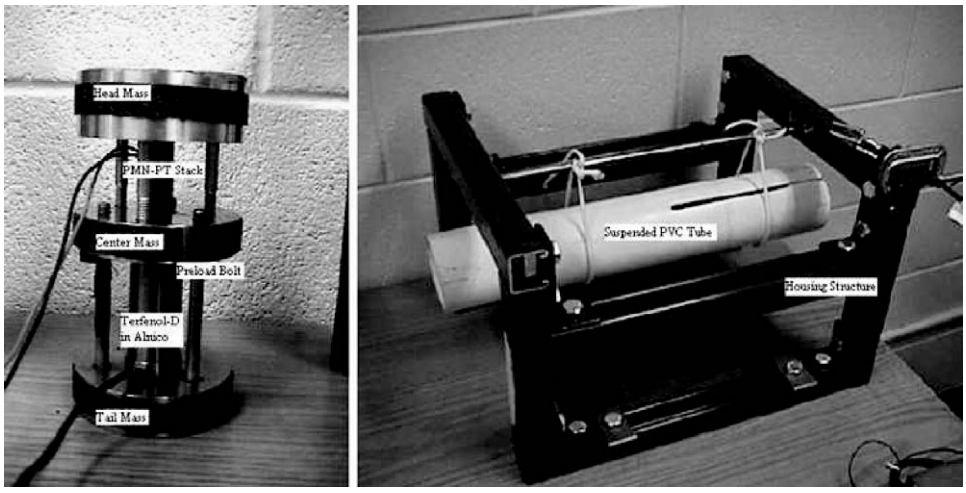

(a) (b)

Figure 8. *(a) Complete hybrid broadband transducer and (b) test structure used for simulation of underwater loading.*

dynamics from affecting the data. Following Butler et al. (1990), the loading effects of water were simulated by filling the PVC tube with duct seal on the radiating face of the head mass.

Low frequency tests were conducted independently on the Terfenol-D and PMN-PT elements to determine the quasistatic linear coupling coefficients q and d, and to find an adequate low signal range so as to avoid unloading of the drivers during dynamic operation. The strain versus magnetic field 'butterfly' curve of the Terfenol-D rod was measured with a linear variable differential transducer (LVDT), and from it a magnetic bias and AC drive level were chosen to limit motion to the steepest linear region on the curve. All subsequent testing employed this magnetic bias, which has a value of 17.6 kA/m. Broadband tests were conducted using white noise excitation with an upper frequency span ranging 5–20 kHz and AC 0-pk drive fields of 15.2 kA/m and 7000 V/m, respectively for the Terfenol-D and PMN-PT sections. The measured quantities in these tests include applied voltage and current, and acceleration at each mass. Tests were conducted with each individual section driven independently and with the two wired in parallel. Additional tests were conducted with a capacitor wired in parallel with the transducer for the purpose of determining the effect of transducer capacitance on the electrical resonance frequency.

DYNAMIC RESULTS AND DISCUSSION

Terfenol-D Section

In all tests of the Terfenol-D section, the voltage excitation was applied across the terminals of the magnetic drive coil while the PMN-PT section was left as an open circuit. In the measurements shown in Figures 9–11, the transducer was driven with no external load. Figure 9 shows the head mass velocity response being dominated by the Terfenol-D section's resonance peak. The modeled data in this case is from the full linear transducer description. The excited motion of the PMN-PT mode is significant, and appears at a frequency in the experimental data slightly higher than in the model simulation. This is due to the open circuit configuration of the piezoceramic stack causing an increase in its stiffness. As the model uses values obtained from the complete closed circuit transducer, it fails to account for this shift.

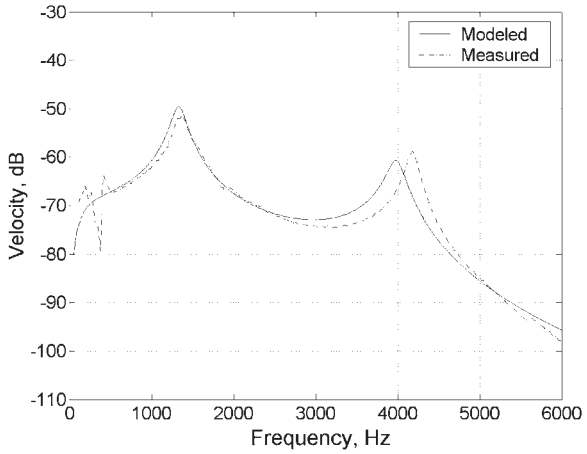

Figure 9. *Head mass velocity response with only Terfenol-D excitation.*

The magnitude of the electrical impedance function Z_{ee} corresponding to this case is shown in Figure 10. Both simulation and data show the anticipated linear increase of Z_{ee} with frequency due to the inductive nature of the solenoid. The coupled motional effects near 1300 Hz agree with the Terfenol-D resonant frequency obtained in the velocity response, while the

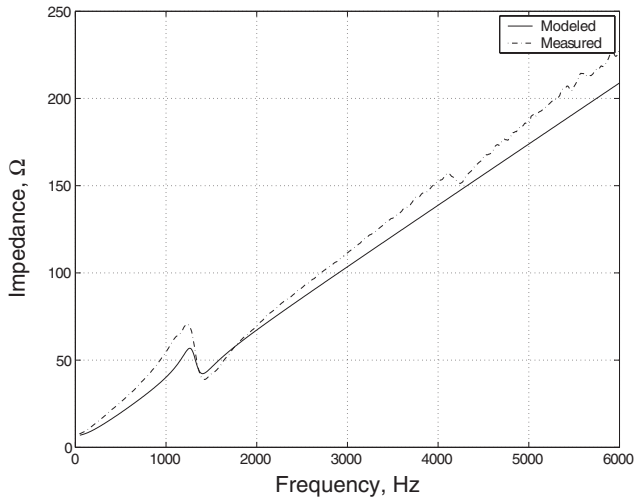

Figure 10. *Electrical impedance magnitude with only Terfenol-D excitation.*

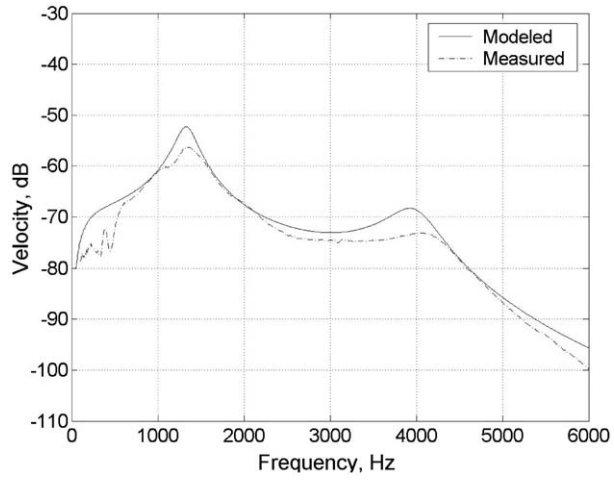

Figure 12. *Head mass velocity response with only Terfenol-D excitation and external load Z_L.*

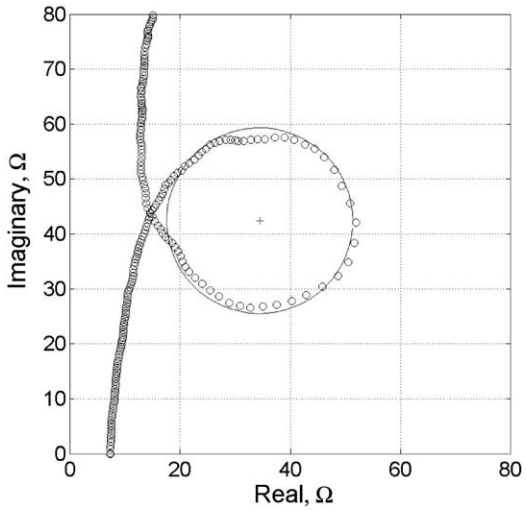

Figure 11. *Impedance mobility loop with only Terfenol-D excitation.*

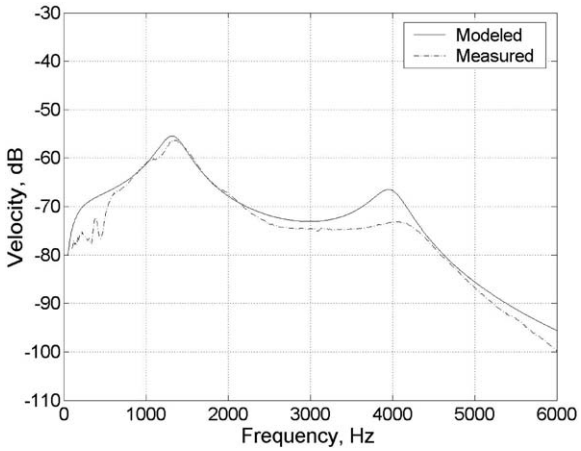

Figure 13. *Head mass velocity response with only Terfenol-D excitation with external load and increased damping in the modeled load impedance.*

measured impedance also shows smaller effects from the excited PMN-PT motion at 4100 Hz. The circular mobility loop in Figure 11 represents the same electrical impedance behavior plotted in Nyquist form. The location of the loop in the first quadrant is indicative of the electrically inductive nature of magnetostrictive transducers while the diameter and roundness are measures of the stiffness and damping present in the transduction.

Similar measurements carried out with the transducer connected to the duct seal loading are shown in Figures 12–15. With identical drive conditions, the presence of radiation impedance adds a Z_{L} term to the existing form of the mechanical impedance, which results in increased damping. This is apparent in the head mass velocity response shown in Figure 12. It is noted that whereas the model accurately predicts the level of damping in the unloaded case, it underestimates the damping in the mechanically loaded case. Figure 13 shows that adding damping in the amount of 600 Ns/m (about a 100% increase) to the modeled load impedance can compensate for this and bring the modeled Terfenol-D resonance right onto the measured data. The need for additional damping in the model may be explained by Equations (17)–(18) being an approximation best suited for lightly damped systems (Meirovitch, 2001). For continuity, all further graphs with the external load include the additional damping term.

The electrical impedance magnitude in Figure 14 shows that for the loaded case, the coupled motional effects are diminished due to the increased damping. The effective coupling coefficient has decreased from 0.44 measured in the unloaded case to 0.33. It is noted, however, that the coupling estimate (14) decreases in accuracy as the damping increases. The mobility loop in Figure 15 is smaller than in the unloaded case and takes on a teardrop shape as a result of the increased losses.

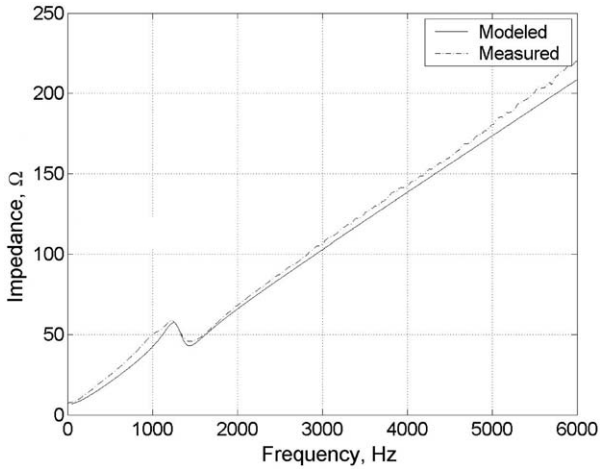

Figure 14. *Electrical impedance magnitude with only Terfenol-D excitation and external load.*

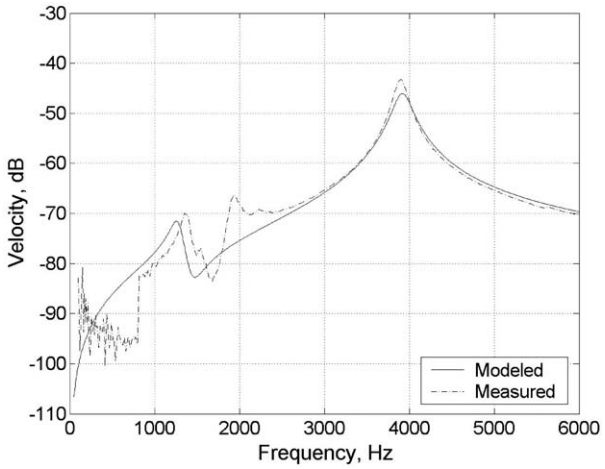

Figure 16. *Head mass velocity response with only PMN-PT excitation.*

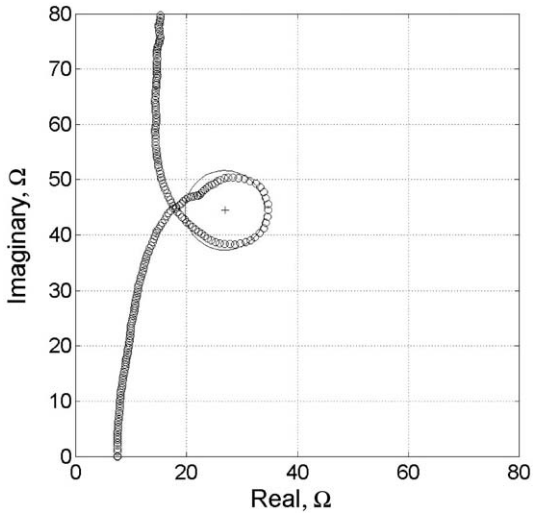

Figure 15. *Impedance mobility loop with only Terfenol-D excitation and external load.*

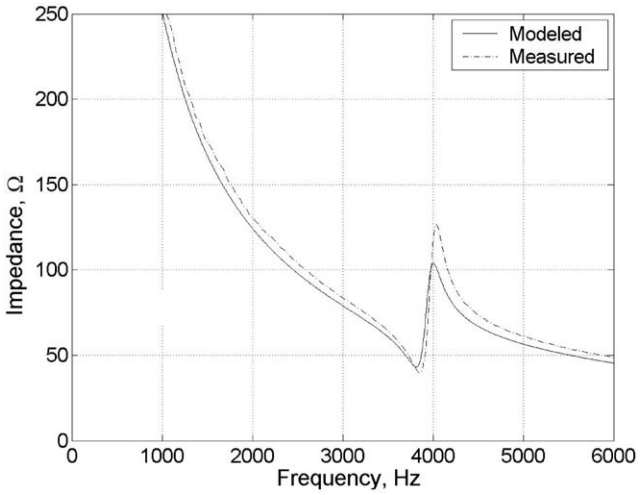

Figure 17. *Electrical impedance magnitude with only PMN-PT excitation.*

PMN-PT Section

In these tests, the PMN-PT section was activated while the magnetic drive coil was left as an open circuit. Unloaded responses are shown in Figures 16–18, while the loaded behaviors are shown in Figures 19–21. The unloaded velocity response in Figure 16 shows the expected high frequency resonance near 3900 Hz. The off-mode effects of the Terfenol-D section appear at a higher frequency than predicted by the model due to the increased stiffness of the open circuit. The magnitude of the electrical impedance in Figure 17 shows the inverse relationship to frequency, consistent with the stack's capacitive properties. The pronounced motional impedance effects are found in Figure 18 to result in a nearly perfectly shaped circular loop, which implies that in this particular transducer the piezoelectric transduction process is cleaner and more efficient than in the magnetostrictive counterpart. The loop is located in the fourth quadrant because the capacitive impedance can be written $1/j\omega C = -j/\omega C$, placing it along the negative imaginary axis.

When the external load impedance is included, the same trends as in the Terfenol-D section are observed. The head mass velocity response for the mechanically loaded case is plotted in Figure 19. Figures 20–21 show that the mechanical loading causes a drastic reduction on the magnitude of the motional effects, and correspondingly on the size and circular quality of the impedance mobility loop.

Complete Transducer

When the two sections are wired in parallel and driven with the same white noise excitation (0−4.2 V rms), the two resonant peaks overlap to successfully extend the

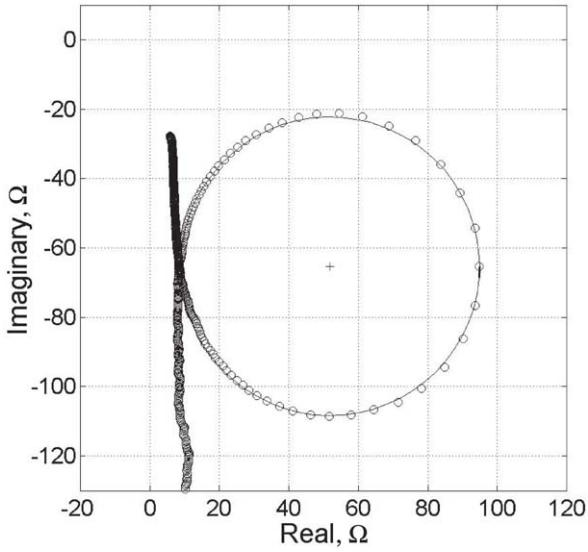

Figure 18. *Impedance mobility loop with only PMN-PT excitation.*

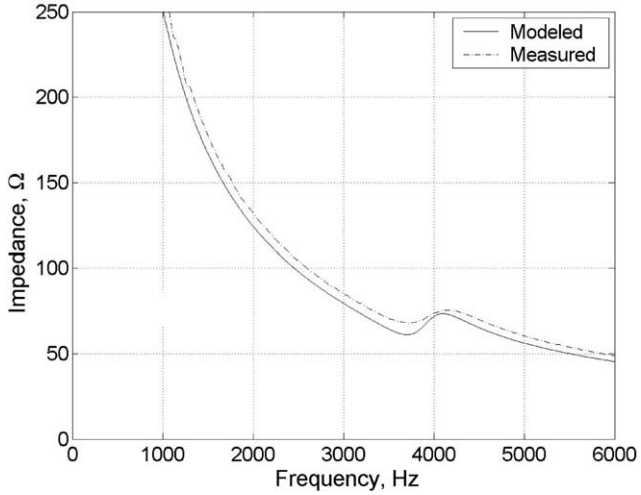

Figure 20. *Electrical impedance magnitude with only PMN-PT excitation and external load.*

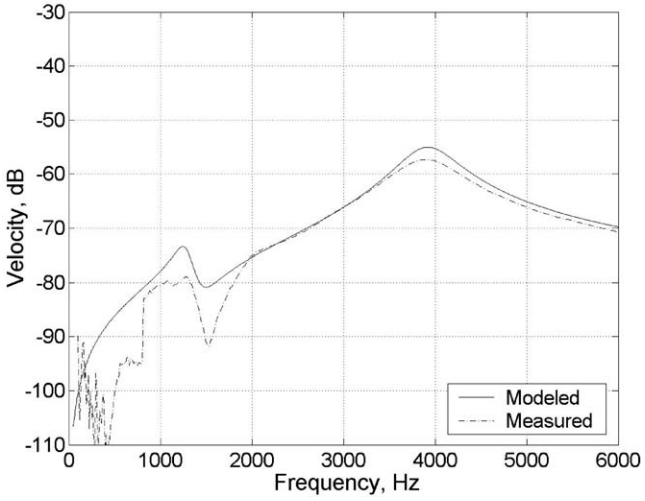

Figure 19. *Head mass velocity response with only PMN-PT excitation and external load.*

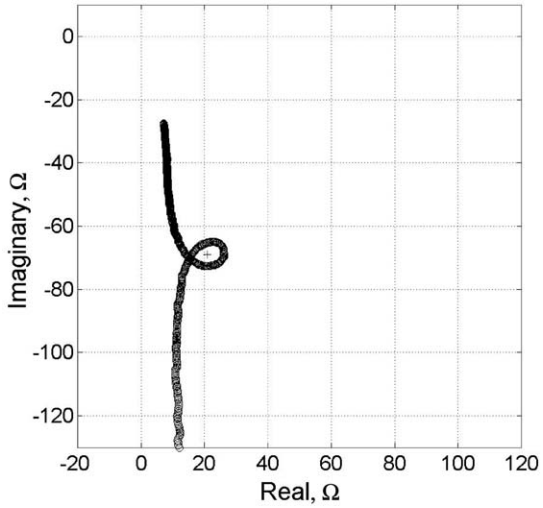

Figure 21. *Impedance mobility loop with only PMN-PT excitation and external load.*

transducer bandwidth to the range 0.5–6 kHz. The head mass velocity response shown in Figure 22 suggests that although the measured peaks overlap accurately with the modeled response, the lack of significant damping creates a large magnitude variation over the frequency range of interest thus resulting in a poor overall frequency bandwidth. Driving the transducer against the duct seal loading adds the damping necessary to achieve a flatter response and improved bandwidth, as illustrated by the velocity response plot of Figure 23.

We also characterized experimentally the effect that tuning the electrical resonance has on the transducer bandwidth. The electrical impedance magnitude shown in Figure 24 corresponds to the same measurement as the velocity response of Figure 23. The Terfenol-D section is shown to behave normally, that is its impedance shows an overall increase with increasing frequency, but the PMN-PT section's resonance is located just to the left of the electrical resonance frequency $\omega_{n,e} = 1/\sqrt{LC}$. As a result, the motional effects are quite large, and the electromechanical coupling k_1 is improved relative to the PMN-PT only case. However, Figure 25 illustrates that the PMN-PT element's mobility loop is located in the first quadrant, before the electrical resonance frequency at the real axis-intercept. This means that the capacitive stack is behaving inductively in this configuration, thus eliminating the benefits of the capacitive/inductive electrical system. Wiring an external 378 nF capacitor in parallel with the circuit changes the effective capacitance and thus shifts the electrical resonant frequency to in between the two mechanical resonances, as shown in Figure 26. The electrical impedance magnitude is now indicative of the two individual modes, as the Terfenol-D section is inductive and the

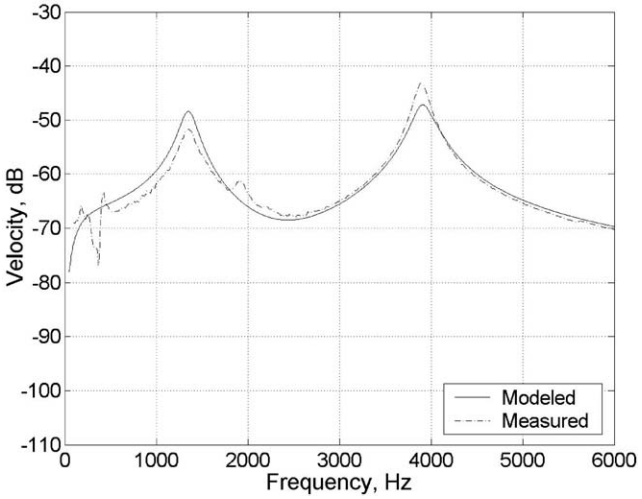

Figure 22. Head mass velocity response with both sections driven.

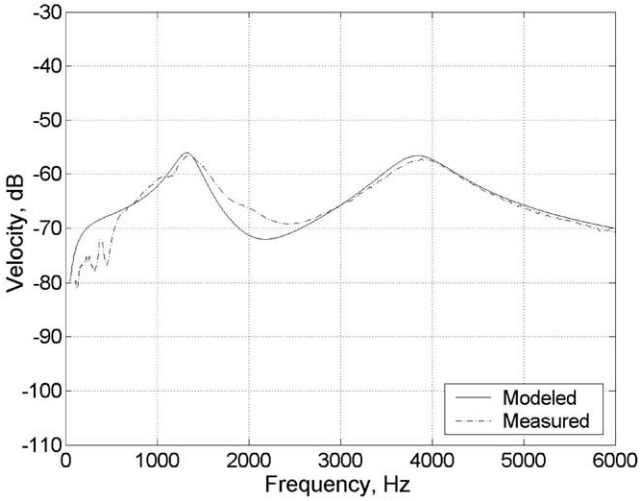

Figure 23. Head mass velocity response with both sections driven and external load.

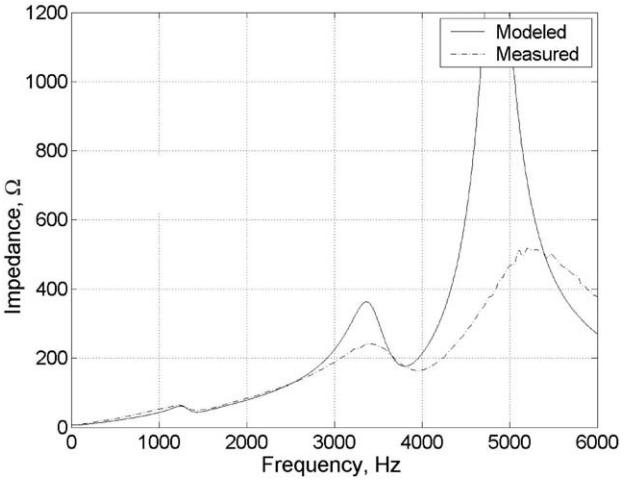

Figure 24. Electrical impedance magnitude with both sections driven and external load.

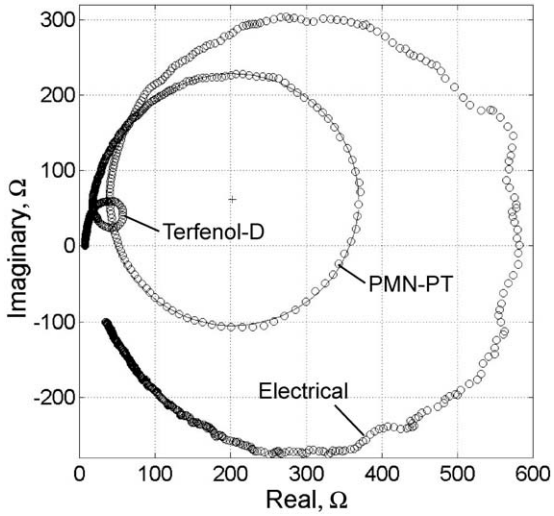

Figure 25. Impedance mobility loop with both sections driven.

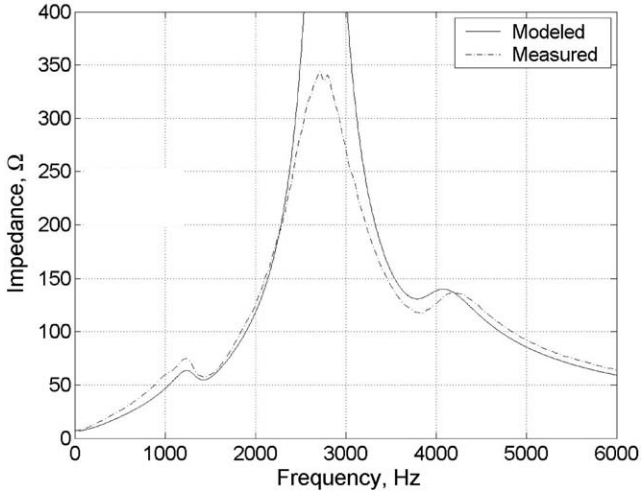

Figure 26. Electrical impedance magnitude with both sections driven with external load and added 378 nF capacitor.

PMN-PT section is once again capacitive. Furthermore, the electrical impedance of the PMN-PT stack has decreased from 240 Ω to 140 Ω. The Nyquist plot in Figure 27 illustrates that the two sections resonate in their original quadrants. The most important result lies in the head mass velocity response, where comparison of Figure 28 versus Figure 23 reveals that altering the electrical resonance leaves the transducer bandwidth essentially unaffected. The latitude for tuning the device capacitance can be regarded as an additional degree of freedom, which can be used to electrically tune the transducer when an existing driver is replaced by a new one due to maintenance or performance reasons, or to individually adjust the transducer response to the properties of a given stack.

It is noted that the frequency bandwidth of the head velocity response shown in Figure 28 is found to have a

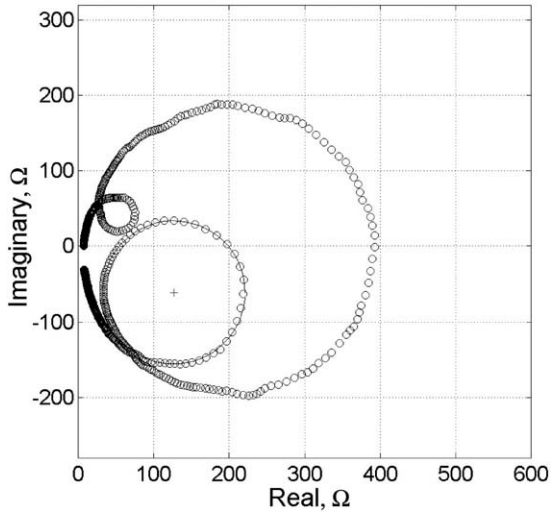

Figure 27. *Impedance mobility loop with both sections driven and added 378 nF capacitor.*

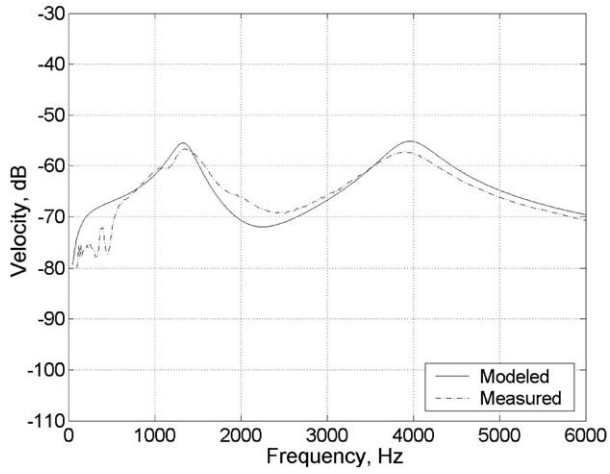

Figure 28. *Head mass velocity response with both sections driven with external load and added 378 nF capacitor.*

magnitude deviation of about 12 dB over the frequency range of interest. Although this would be considered too large a variation for effective use, Tonpilz transducers are typically incorporated into array structures which exhibit enhanced bandwidth relative to the individual elements. A US navy prototype of a similar hybrid architecture has been shown to exhibit a comparable decibel variation over the bandwidth of a single element, but only a 3 dB variation when configured in a 4×4 transducer array (Butler and Tito, 2000).

CONCLUDING REMARKS

Despite the general limitations of linear models when applied to materials that exhibit nonlinearities and hysteresis, such models are justified in this study by the consideration of biased, low signal regimes in which transducer behavior is quasilinear. Furthermore, unlike in the previous studies we consider a ferroelectric driver, made of lead magnesium niobate doped with lead titanate, which exhibits a high degree of strain linearity when operated near room temperature. The model is shown to present several advantages. It provides simulations of electrical and mechanical transducer behavior which are sufficiently accurate for design and control applications while being simple to implement. The principles employed to construct the model are classical and widely available in the open literature. The model also provides a framework for material property characterization, that is, the same dynamic equations employed for analysis of the transducer give when combined with electrical impedance and velocity measurements, the material parameters of the ferroelectric and ferromagnetic elements. This dynamic characterization method is considered advantageous over the conventional approach of deriving material properties from quasistatic measurements based on butterfly curves, for the latter approach yields inaccurate results when the parameters are employed in dynamic transducer equations. In addition to demonstrating excellent bandwidth characteristics from the hybrid Terfenol-D/PMN-PT device, we show that it is possible to electrically tune the device without fundamentally affecting its frequency bandwidth. This provides an additional degree of freedom for adjusting the transducer response to ferroelectric drivers of various capacitances.

ACKNOWLEDGMENTS

The authors gratefully acknowledge Julie Slaughter (Etrema Products, Inc.) for providing Terfenol-D samples as in-kind contribution to this investigation, and Stephen Butler (Naval Undersea Warfare Systems Division Newport) for useful discussions. Funding was provided by Ohio State University through a start up grant.

REFERENCES

Butler, J.L. and Clark, A.E. 1984. "Hybrid Piezoelectric and Magnetostrictive Acoustic Wave Transducer," US Patent No. 4,443,731, 17 April 1984.

Butler, J.L., Butler, S.C. and Clark, A.E. 1990. "Unidirectional Magnetostrictive/Piezoelectric Hybrid Transducer," *Journal of the Acoustical Society of America*, 88(1):7–11.

Butler, J.L., Butler, A.L. and Butler, S.C. 1993. "Hybrid Magnetostrictive/Piezoelectric Tonpilz Transducer," *Journal of the Acoustical Society of America,* 94(2):636–641.

Butler, S.C., Lindberg, J.F. and Clark, A.E. 1996. "Hybrid Magnetostrictive/Piezoelectric Tonpilz Transducer," *Ferroelectrics*, 187(1–4):163–174.

Butler, S.C. 1998. "A Broadband Hybrid Magnetostrictive/Piezoelectric Tonpilz Transducer," In: *Undersea Defence Technology Conference, UDT Pacific 98*, Sydney, Australia.

Butler, S.C. and Tito, F.A. 2000. "A Broadband Hybrid Magnetostrictive/Piezoelectric Transducer Array," *OCEANS 2000 MTS/IEEE Conference and Exhibition*, 3:1469–1475.

Dapino, M.J., Flatau, A.B. and Calkins, F.T. "Statistical Analysis of Terfenol-D Material Properties," *Journal of Intelligent Material Systems and Structures* (to appear).

Downey, P.R., Dapino, M.J. and Smith, R.C. 2003. "Analysis of Hybrid PMN/Terfenol Broadband Transducers in Mechanical Series Configuration," In: *Proceedings of SPIE Smart Structures and Materials*, Vol. 5049, San Diego, CA, pp. 168–179.

Hall, D. 1994. "Dynamics and Vibrations of Magnetostrictive Transducers," PhD Thesis, Iowa State University.

Hunt, F.V. 1982. *Electroacoustics: The Analysis of Transduction, and Its Historical Background*, American Institute of Physics for the Acoustical Society of America.

Janocha, H. and Clephas, B. 1996. "Hybrid Actuator with Piezoelectric and Magnetostrictive Material," In: *ACTUATOR 96, Proc. 5th International Conference on New, Actuator*, Axon Technologie Consult GmbH, Bremen, Germany, pp. 304–307.

Meirovitch, L. 2001. *Fundamentals of Vibrations*, McGraw-Hill, Boston.